

Article

Structure–Phase Transformations in the Modified Surface of Al-20%Si Alloy Subjected to Two-Stage Treatment

Yulia Shliarova ¹, Dmitrii Zaguliaev ^{1,*} , Yurii Ivanov ², Victor Gromov ¹  and Alexander Prudnikov ¹

¹ Natural Sciences Department, Siberian State Industrial University, 654007 Novokuznetsk, Russia; rubannikova96@mail.ru (Y.S.); gromov@physics.sibsiu.ru (V.G.); a.prudnikov@mail.ru (A.P.)

² Institute of High Current Electronics SB RAS, 634055 Tomsk, Russia; yufi55@mail.ru

* Correspondence: zagulyaev_dv@physics.sibsiu.ru

Abstract: The paper describes the two-stage modification of the surface layer of hypereutectic Al-20%Si alloy that combines electroexplosive alloying by an Al-Y₂O system with subsequent irradiation by pulsed electron beam. It is shown that irrespective of the modification mode, a multilayer structure is formed consisting of the following layers: a surface layer and an intermediate layer. The surface layer is a multiphase material, the thickness of which varies within 1 μm. The intermediate layer, the thickness of which varies within 40 μm, is made up of rapid solidification cells formed due to the rapid cooling of molten layer of Al-20%Si alloy. The cells are divided by thin interlayers mostly formed by silicon nanoparticles.

Keywords: Al-20%Si alloy; pulsed electron beam; microstructure; surface layer; modification



Citation: Shliarova, Y.; Zaguliaev, D.; Ivanov, Y.; Gromov, V.; Prudnikov, A. Structure–Phase Transformations in the Modified Surface of Al-20%Si Alloy Subjected to Two-Stage Treatment. *Lubricants* **2022**, *10*, 133. <https://doi.org/10.3390/lubricants10070133>

Received: 25 February 2022

Accepted: 14 June 2022

Published: 22 June 2022

Publisher's Note: MDPI stays neutral with regard to jurisdictional claims in published maps and institutional affiliations.



Copyright: © 2022 by the authors. Licensee MDPI, Basel, Switzerland. This article is an open access article distributed under the terms and conditions of the Creative Commons Attribution (CC BY) license (<https://creativecommons.org/licenses/by/4.0/>).

1. Introduction

Currently, the modern machine-building industry faces a large number of challenges: the development of new materials or materials with improved properties; the introduction of new technologies; energy and resources saving through the production of economical and efficient materials for machines and manufacturing equipment; improvement of reliability and the service life of products, etc. In most cases, during the operation of machine parts and mechanisms, it is the surface layers of material that are subjected to the load, and that is why they attract the maximum attention of scientists [1–4].

The service life of machine parts during their operation is reduced, and the performance deterioration takes place irreversibly because of wear and damage to parts. Every year, millions of parts are rejected and remelted due to the wear-out of their working surfaces, which can be recovered by different methods. The cost of parts recovery is much lower than their manufacturing cost, as recovery does not include such labor-, energy- and material-intensive processes as remelting (when recycling the worn-out item), casting, stamping and machining (when producing a new item). In many cases, the solution of these problems is facilitated by the wide use of aluminum alloys in industry, the development and introduction of resource-efficient technologies of their production, and the creation of new constructional and precision materials with pre-designed properties [5–7].

It is known that 80% of aluminum castings produced in the world are made of aluminum–silicone (Al–Si) alloys—silumins. A specific feature of silumins, as opposed to pure aluminum, is their increased strength and hardness, wear and corrosion resistance resulting from the content of silicone, which is harder than aluminum [8]. This explains the idea of developing and using the hypereutectic silumin in which the content of silicone exceeds ≈12 wt %. However, the presence of such an amount of silicone conditions the large inclusions, pores, cracks, etc., in silumin, reducing the performance properties of the material [9–13].

Pistons for automobiles are most often produced from eutectic and hypereutectic silumins with silicone content of 12–25 wt %. Modification and microalloying are known to influence greatly the improvement of performance and stress-related characteristics of these alloys [14–18]. The piston operates under rough, often dangerous, conditions—rubbing friction, increased temperature modes and intense loads; that is why it is especially important for the automobile pistons to be efficient, reliable and wear resistant. Thus, there is a need for rubbing surface protection. It is achieved by the methods of surface hardening. The interaction of intense pulse energy beams, such as ion, electron and laser beams, with materials and its application in industry has drawn great attention in recent decades.

Currently, the most promising method of metals and alloys surface treatment is two-stage processing, which combines a complex of treatment methods: surfacing and subsequent radiation treatment by an electron beam. The given combination of methods allows not only the thermal action upon the material surface to be implemented but also the alloying of the surface layer to be performed [19,20]. All of the above-mentioned methods acting upon the structure and the phase composition allow the greater part of the disadvantages to be minimized and the service life of machine parts and mechanical components to be increased.

Thus, the treatment of the surface layers of hypereutectic silumins is a challenging issue for the modern machine-building industry. In this regard, the aim of this paper is to analyze the structure–phase transformations taking place in the surface layer of hypereutectic alloy Al-20%Si subjected to the two-stage treatment.

2. Materials and Methods

The samples of hypereutectic alloy Al-20%Si were used as a material for study. The chemical composition obtained after X-ray diffraction analysis (Shimadzu XRF-1800 instrument) of silumin samples is shown in Table 1.

Table 1. Results of X-ray spectrum analysis of Al-20Si alloy samples.

Al	Si	Fe	Cu	Mn	Ni	Ti	Cr
78.52 ± 10%	20.28 ± 10%	1.14 ± 10%	0.072 ± 10%	0.015 ± 10%	0.006 ± 10%	0.006 ± 10%	0.001 ± 10%

Modification of the silumin surface layer was performed in two stages. At the first stage, electroexplosive alloying of Al-20%Si was completed, aluminum foils were used as the material for exploding conductors, and Y₂O₃ was used as the sample weight. Alloying was carried out at the electrical discharge machine EVU 60/10 [21].

Coating was carried out according to the following technology: the sample weight of Y₂O₃ powder was placed on the aluminum foil gripped between two coaxial electrodes. Then, voltage was applied to the foil through the vacuum gap, the conductor, exposed to high-density current, exploded. Explosion products, which consisted of the plasma component including variously dispersed particles of Al and Y₂O₃ moved along the process chamber to the sample, were deposited on it with fusion of the material surface layers. Thus, the multiphase and multicomponent coating was formed on the surface of the treated part.

At the second stage, the modified surface was irradiated by a pulsed electron beam. The irradiation was completed at the energy complex “SOLO” developed and produced in the Institute of High Current Electronics SB RAS (Tomsk) [22]. The irradiation was performed in the atmosphere of argon under the pressure of 0.02 Pa. The conditions of electroexplosive alloying and subsequent alloy irradiation are presented in Table 2. Earlier in paper [23], the authors analyzed six modes of treatment and determined the optimal conditions of electroexplosive alloying, resulting in multiple increases in the mechanical characteristics of the alloy surface layer.

Table 2. The conditions of electroexplosive alloying and subsequent treatment by electron beam.

Mode No.	Mass of the Aluminum Foil, m_{Al} (mg)	Mass of the Powder Y_2O_3 , $m_{Y_2O_3}$ (mg)	Discharge Voltage, U (kV)	Electron Beam Energy Density, J/cm^2	Energy of Accelerated Electrons, keV	Duration of Electron Beam Pulse, μs	Number of Current Pulses	Pulse Repetition Rate, s^{-1}
1	58.9	58.9	2.8	35	18	150	3	0.3
2	58.9	88.3	2.6	25				

Study of the phase composition and structural parameters of the samples was performed by the methods of X-ray structure analysis (X-ray diffraction meter XRD-6000 on $CuK\alpha$ -radiation). Analysis of the phase composition was performed with the application of databases PDF 4+ and full-profile analysis POWDER CELL 2.4. The defective substructure, morphology and local phase composition of the modified layer of silumin samples was carried out by the methods of transmission electron diffraction microscopy (unit JEM 2100F) [24–26].

3. Results

The morphology of the modified layer of Al-20%Si alloy was studied by the method of transmission electron microscopy of foils prepared from the plates cut out of the bulk samples perpendicularly to the treated surface. In Figure 1, we provide the typical image of the layer structure formed after the two-stage treatment. It was established that regardless of the modification mode, a multilayer structure is formed: the surface layer (Figure 1a, layer I) and the intermediate layer (Figure 1a, layer II).

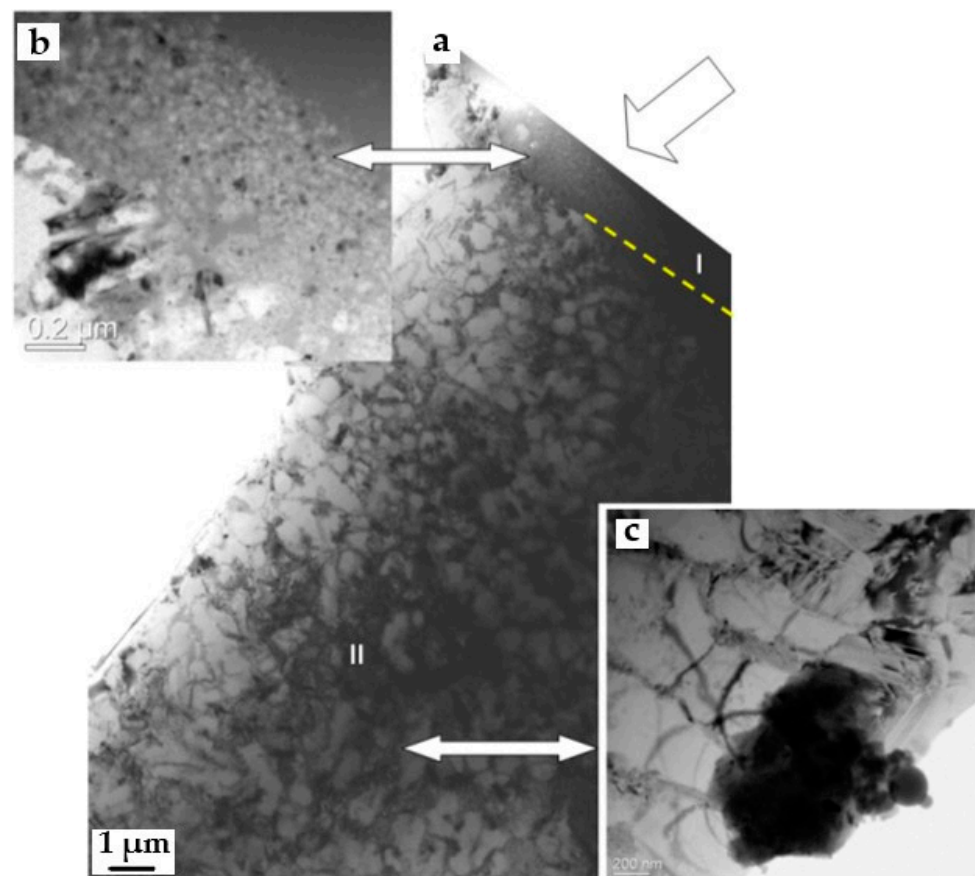


Figure 1. Structure of the surface layer of Al-20%Si alloy modified by the two-stage treatment. (a) a multilayer structure: the surface layer (layer I) and the intermediate layer (layer II); (b) the surface layer structure; (c) the intermediate layer structure.

Surface layer I is formed by circular-shaped particles, the sizes of which vary within $\approx 10\text{--}20$ nm (Figure 1b). The thickness of the given layer varies within ≈ 1 μm . We can suppose that the given particles are yttrium oxide powder or yttrium oxide powder modified as a result of its interaction with the molten surface layer of the base. The intermediate layer (layer II) has the structure of rapid cellular solidification, which is a typical structure for silumin treated by pulse electron beam in the mode of surface layer fusion [27,28]. The given layer is characterized by globular inclusions formed by circular nanoparticles (Figure 1c). We can suppose that these inclusions are conglomerates of yttrium oxide particles. The thickness of the given layer is 30–40 μm , and it increases as the energy density of the electron beam grows.

The phase composition and the crystalline lattice of the main phases were studied by the methods of X-ray diffraction analysis. The results of the X-ray diffraction analysis of Al-20%Si alloy subjected to the two-stage treatment are presented in Table 3.

Table 3. Results of X-ray diffraction analysis of Al-20%Si alloy subjected to the two-stage treatment.

Sample	Determined Phases	Phase Content, Mas. %	Lattice Constant, \AA	Size of the Coherent Scattering Region, nm	$\Delta d/d \cdot 10^{-3}$
No. 1–35 J/cm ²	Al(Si)	73.0	a = 4.0509	94.3	0.761
	Si	16.8	a = 5.4437	16.27	1.026
	Y ₂ O ₃	3.8	a = 10.5080 a = 3.8995	24.09	7.588
	YSi ₂	6.4	b = 4.1392 c = 13.2821	18.59	2.142
No. 2–25 J/cm ²	Al(Si)	71.5	a = 4.0516	320.53	1.853
	Si	25.9	a = 5.4341	41.92	1.589
	Y ₂ O ₃	2.6	a = 10.5871	13.8	2.509

Analyzing the results presented in Table 3, we can note that the phase composition and the condition of the crystalline lattice of the main phases significantly depend on the conditions of modification. From the reference books, it follows that aluminum and silicone are practically insoluble in one another in the room temperature [29]. Consequently, we can take the lattice constant of pure aluminum which equals 0.4046 nm as the lattice constant of aluminum in the base alloy Al-20%Si [29]. The two-stage treatment of Al-20%Si alloy results in an increase in the lattice constant of aluminum, and this may indicate that aluminum was alloyed by yttrium atoms as the radius of yttrium atoms ($R(\text{Y}) = 0.178$ nm) is larger than the radius of aluminum atoms ($R(\text{Al}) = 0.143$ nm). The size of the coherent scattering regions and the ratio of the aluminum lattice microdistortions are larger in sample No. 2. It can be conditioned by the greater concentration of yttrium oxide powder introduced into the silumin surface layer during the electroexplosive alloying.

The content of silicone in the silumin surface layer is reduced by 1.5 as the energy density of the electron beam increases. This reduction may result from the transition of some part of crystalline silicone into amorphous silicone under high-speed thermal treatment. The silicone lattice constant grows when the energy density of electron beam increases and in both cases exceeds the pure silicone lattice constant, which equals 0.54304 nm [29]. The latter can be conditioned by the alloying of silicone with yttrium and aluminum atoms, as the radius of silicone atoms ($R(\text{Si}) = 0.134$ nm) is smaller than the radius of aluminum and yttrium atoms. The size of the coherent scattering regions and the ratio of the silicone lattice microdistortions are larger in sample No. 2. This can be determined by the greater concentration of yttrium oxide powder introduced into the surface layer of silumin during the electroexplosive alloying.

As it was mentioned above, the modified layer of Al-20%Si alloy contains yttrium oxide powder. This powder is also detected by the methods of X-ray diffraction analysis (Table 3). Its content ratio is relatively small and varies within 2.8–3.6 mass %. The lattice constant of the yttrium oxide is reduced as the energy density of the electron beam grows. Let us note that the lattice constant of yttrium oxide crystalline lattice was 1.061 nm [29]. The microdistortions of the crystalline lattice of yttrium oxide change significantly: they increased three times when the energy density of the electron beam grows from 25 to 35 J/cm² (Figure 2). The microdistortions of the crystalline lattice of Al and Si phases change in the opposite way: they are reduced when the energy density of the electron beam increases.

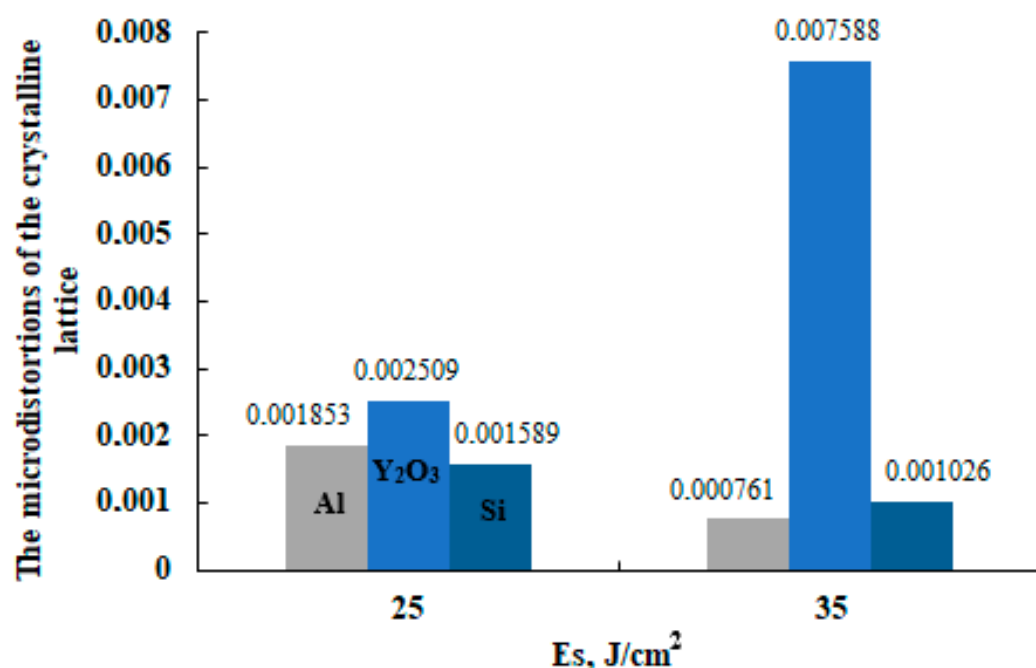


Figure 2. Dependence of the microdistortions of the crystalline lattice on the energy density of the electron beam for Al-20%Si alloy.

Irradiation of the surface layer of Al-20%Si alloy, modified by the electroexplosive method with subsequent irradiation by pulse electron beam with energy density of the electron beam 35 J/cm², leads to the formation of yttrium silicide YSi₂ in the alloy. At the lower energy density of the electron beam, the given compound is not found in the alloy.

The morphology, sizes and phase distribution in the surface layer of Al-20%Si alloy subjected to the two-stage treatment were studied by the methods of transmission diffraction electron microscopy, applying the methods of dark-field analysis and indexing of X-ray diffraction patterns [30,31].

In Figure 3, the results of selected-area electron diffraction analysis of the surface layer are shown (layer I, Figure 1a,b). On the dark-field images of the given layer (Figure 3c,d), it is clearly seen that the layer is a nanostructured formation, and it is formed by circular particles. Indexing of the X-ray diffraction pattern obtained for the given layer (Figure 3b) allowed revealing reflections of the following phases: YAl₃ (indicated by yellow arrows in Figure 3b) and Y₂Si₂O₇ (indicated by red arrows in Figure 3b). Consequently, we can suppose that the given surface layer was formed as a result of the interaction between Y₂O₃ powder and the molten layer of Al-20Si alloy, which led to the formation of the phases of elements in the given layer.

In Figure 4, the electron microscopic image of the intermediate layer structure is presented. It is clearly seen that the given layer is formed by the cells of rapid solidification resulting from rapid cooling of the molten layer. Analysis of the X-ray diffraction pattern brings us to the conclusion that the cells are formed by solid solution on the aluminum base (Figure 4d). The cells are divided by thin interlayers formed by nanosized particles. Indexing of the X-ray diffraction pattern shows that these particles are silicone (Figure 4c). Analyzing the results presented in Figure 4c, it can be noted that the silicon interlayers are formed by aluminum-based solid solution. Silicon interlayers are located along the boundaries and at the junctions of the boundaries of the crystallization cells and have a nanocrystalline structure with a crystallite size of $\approx 10\text{--}20$ nm.

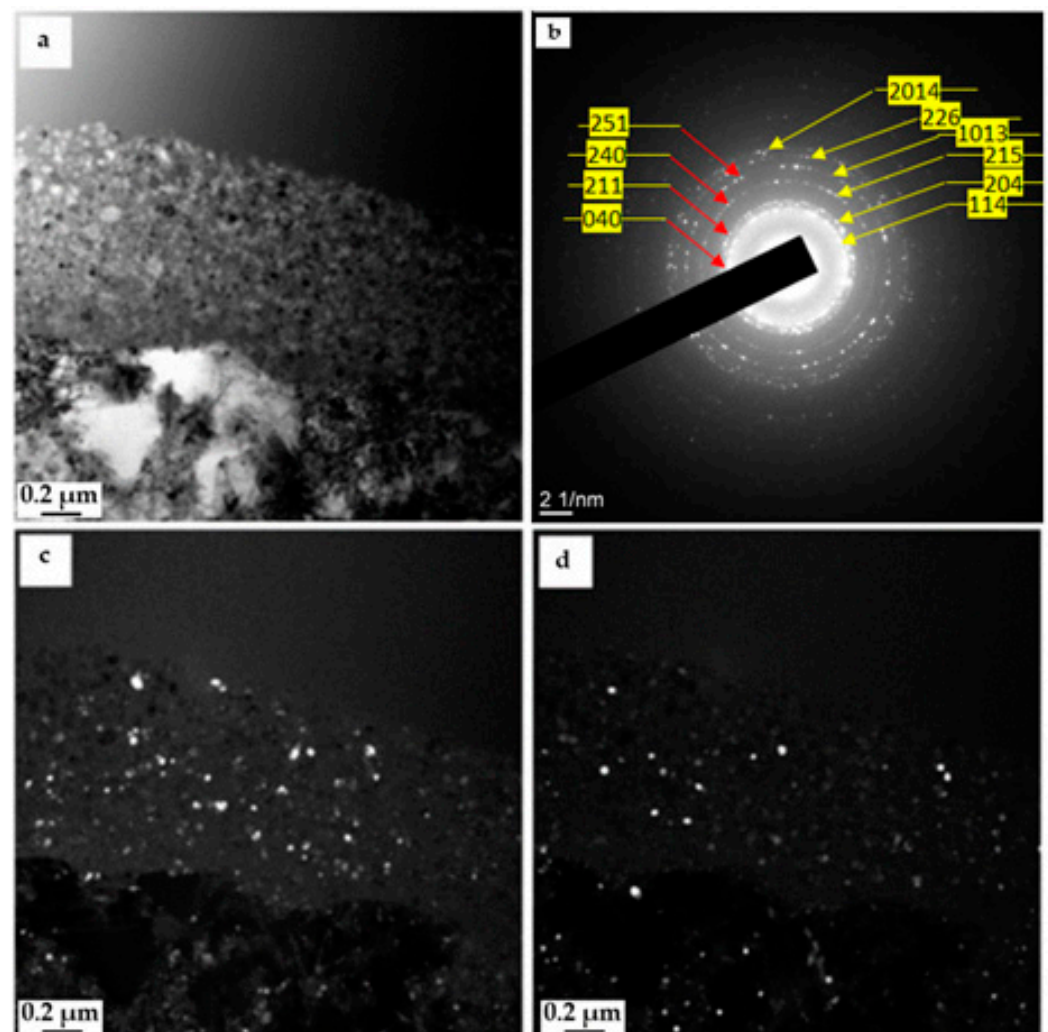


Figure 3. Electron microscopic image of the surface layer structure of Al-20%Si formed as a result of the two-stage treatment which combines electroexplosive alloying by yttrium oxide powder and subsequent irradiation with a pulse electron beam; (a) bright-field; (b) X-ray diffraction pattern; (c,d) dark-field images obtained in reflections [204]YAl₃ and [211]Y₂Si₂O₇ (c); [1013]YAl₃ and [251]Y₂Si₂O₇ (d); in (b) diffraction rings are shown in which dark-field images were obtained: 1—for (c), 2—for (d). Yellow arrows indicate diffraction rings belonging to the YAl₃ phase; red arrows indicate diffraction rings belonging to the Y₂Si₂O₇ phase.

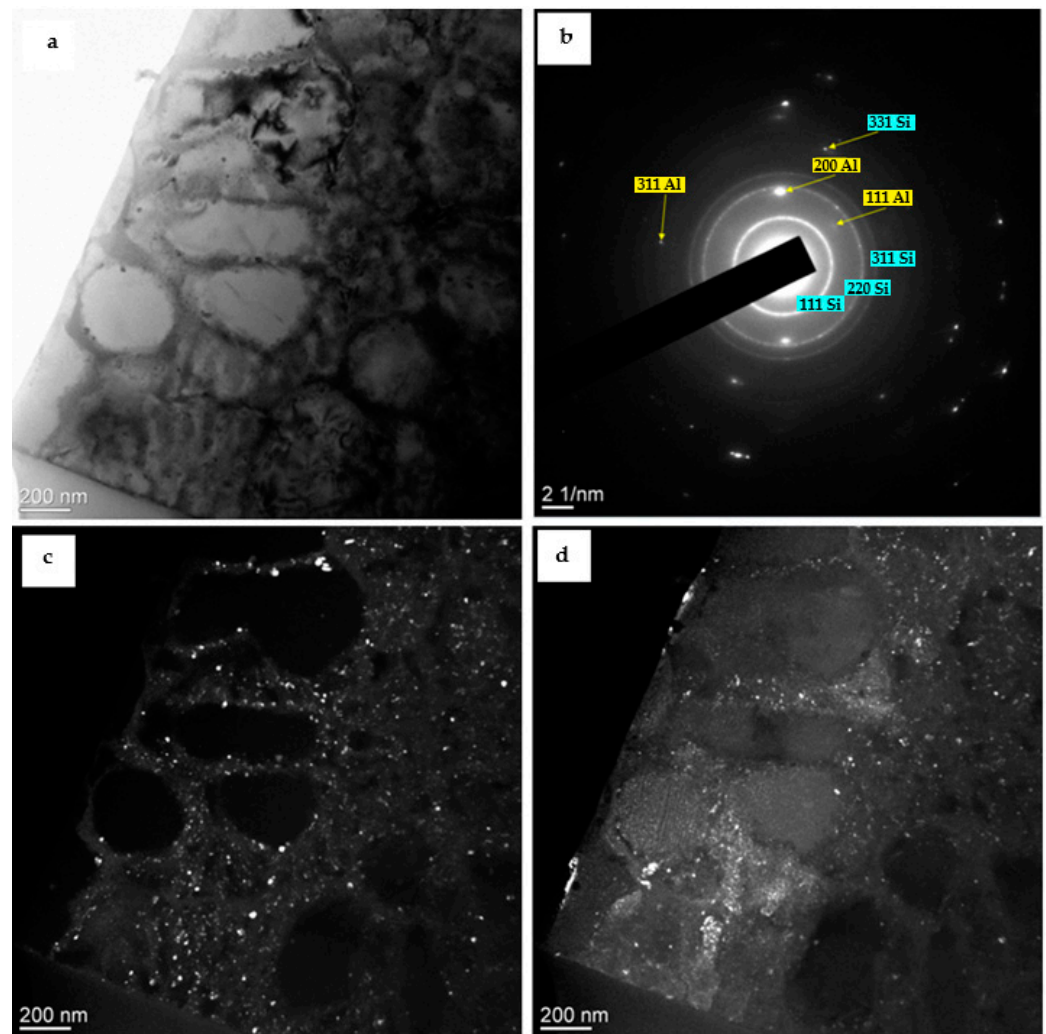


Figure 4. Electron microscopic image of the intermediate layer structure of Al-20%Si formed as a result of the two-stage treatment which combines electroexplosive alloying by yttrium oxide powder and subsequent irradiation with a pulse electron beam; (a) bright-field; (b) X-ray diffraction pattern; (c,d) dark-field images obtained in reflections [220]Si (c) and [200]Al (d).

In Figure 5, an electron microscopic image of the foil area with an agglomerate of spherical particles is provided. Analysis of X-ray diffraction pattern obtained for the given agglomerate allowed the reflections belonging to the crystalline lattice of Y_2SiO_7 compound phase to be revealed (Figure 5b). This indicates that the agglomerates of yttrium oxide powder introduced into the molten layer of Al-20%Si alloy can be alloyed by the elements forming the base material.

Thus, the methods of transmission electronic diffraction microscopy allow not only studying morphology and estimating the size of second phase particles but also revealing additional phases which are not shown by the methods of X-ray diffraction analysis due to their small content in the material.

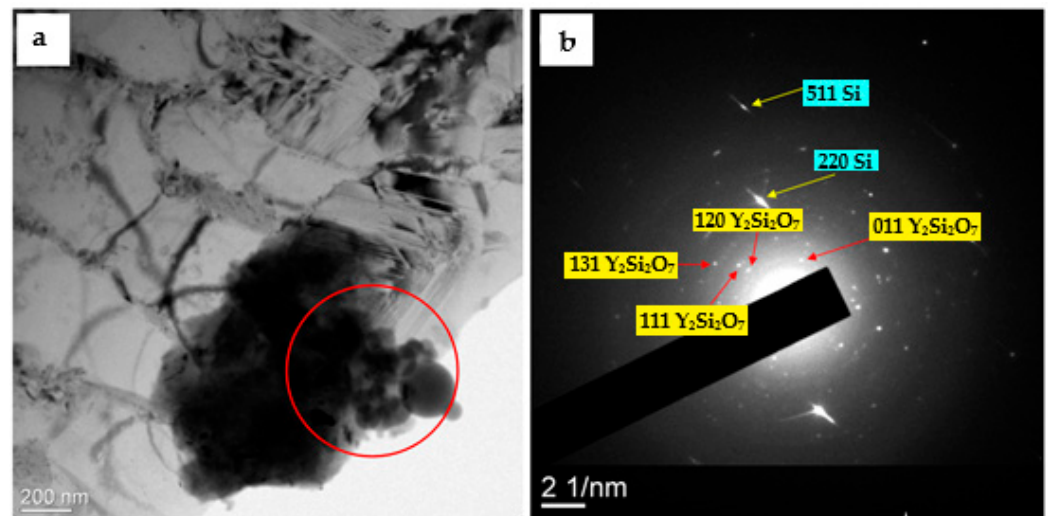


Figure 5. Electron microscope image of the intermediate layer structure of Al-20%Si formed as a result of the two-stage treatment which combines electroexplosive alloying by yttrium oxide powder and subsequent irradiation with a pulse electron beam; (a) bright field; (b) microelectron diffraction pattern obtained from the foil section limited by the selector diagram (red circle in Figure 5a).

4. Conclusions

The structure, the phase composition, and the state of the defective substructure of Al-20%Si alloy samples subjected to the two-stage treatment (electroexplosive alloying with subsequent irradiation by high-intensity pulse electron beam) were studied by the methods of transmission electronic diffraction microscopy. It was established that regardless of the modification conditions, a multilayer structure is formed: the surface layer and intermediate layer. It was shown that the surface layer, the thickness of which is within 1 μm , is a multiphase material and is formed, supposedly, as a result of interaction between Y_2O_3 powder and the molten Al-20%Si layer. The intermediate layer, the thickness of which varies within 40 μm , is made up of rapid solidification cells formed due to the rapid cooling of the molten layer of Al-20%Si alloy. The cells are divided by thin interlayers mostly formed by silicon nanosized particles. It was established that agglomerates of spherical particles are found in the intermediate layer. It was shown that these agglomerates are formed by the yttrium oxide particles introduced into the molten layer of Al-20%Si and alloyed by the elements forming the base material. Solid solutions based on aluminum and silicon crystal lattices enriched with yttrium atoms were revealed in the intermediate layer appearing due to the rapid solidification.

Author Contributions: Conceptualization, D.Z.; methodology, Y.I. and V.G.; formal analysis, Y.S. and A.P.; writing—original draft preparation, D.Z. and Y.S.; writing—review and editing, D.Z.; supervision, V.G.; project administration, Y.S. All authors have read and agreed to the published version of the manuscript.

Funding: The research was financially supported by the Russian Science Foundation (RSF) (project No. 19-79-10059).

Data Availability Statement: The data presented in this study are available on request from the corresponding author.

Conflicts of Interest: The authors declare no conflict of interest.

References

1. Blutmager, A.; Varga, M.; Cihak-Bayr, U.; Friesenbichler, W.; Mayrhofer, P.H. Wear in hard metal check valves: In-situ surface modification through tribolayer formation in dry contact. *Vacuum* **2021**, *192*, 110482. [\[CrossRef\]](#)
2. Jiang, H.; Ren, Z.; Yi, Y.; He, L.; Yuan, S. Effect of machining on performance enhancement of superficial layer of high-strength alloy steel. *J. Mater. Res. Technol.* **2021**, *14*, 1065–1079. [\[CrossRef\]](#)
3. Liu, Z.; Zhang, H.; Yan, Z.; Dong, P. Enhanced fatigue performance of aluminum alloy through surface strengthening treatment. *Mater. Lett.* **2022**, *306*, 130864. [\[CrossRef\]](#)
4. Zhou, J.; Han, X.; Li, H.; Liu, S.; Yi, J. Investigation of layer-by-layer laser remelting to improve surface quality, microstructure, and mechanical properties of laser powder bed fused AlSi10Mg alloy. *Mater. Des.* **2021**, *210*, 110092. [\[CrossRef\]](#)
5. Kagramanian, A.; Stankevich, P.; Aulin, D.; Basov, A. Efficiency improvement of locomotive-type diesel engine operation due to introduction of resource-saving technologies for cleaning diesel and diesel locomotive systems. *Procedia Comput. Sci.* **2019**, *149*, 264–273. [\[CrossRef\]](#)
6. Denkena, B.; Dittrich, M.-A.; Liu, Y.; Theuer, M. Automatic Regeneration of Cemented Carbide Tools for a Resource Efficient Tool Production. *Procedia Manuf.* **2018**, *21*, 259–265. [\[CrossRef\]](#)
7. Fanghänel, C.; Rautenstrauch, A.; Symmank, C.; Katzenberger, J.; Putz, M.; Kräusel, V.; Götze, U.; Awiszus, B. Multidimensional Analysis of Process Chains Regarding the Resource-efficient Manufacturing of Hybrid Structures. *Procedia CIRP* **2015**, *26*, 595–600. [\[CrossRef\]](#)
8. Polmear, I.; StJohn, D.; Nie, J.F.; Qian, M. *Light Alloys: Metallurgy of the Light Metals*, 5th ed.; Butterworth-Heinemann: Boston, MA, USA, 2017; p. 544.
9. Li, R.; Liu, L.; Zhang, L.; Sun, J.; Shi, Y.; Yu, B. Effect of Squeeze Casting on Microstructure and Mechanical Properties of Hypereutectic Al-xSi Alloys. *J. Mater. Sci. Technol.* **2017**, *33*, 404–410. [\[CrossRef\]](#)
10. Jung, J.-G.; Ahn, T.-Y.; Cho, Y.-H.; Kim, S.-H.; Lee, J.-M. Synergistic effect of ultrasonic melt treatment and fast cooling on the refinement of primary Si in a hypereutectic Al–Si alloy. *Acta Mater.* **2018**, *144*, 31–40. [\[CrossRef\]](#)
11. Lu, Z.; Zhang, L.; Wang, J.; Yao, Q.; Rao, G.; Zhou, H. Understanding of strengthening and toughening mechanisms for Sc-modified Al-Si-(Mg) series casting alloys designed by computational thermodynamics. *J. Alloy. Compd.* **2019**, *805*, 415–425. [\[CrossRef\]](#)
12. Cai, Z.; Zhang, C.; Wang, R.; Peng, C.; Qiu, K.; Wang, N. Effect of solidification rate on the coarsening behavior of precipitate in rapidly solidified Al-Si alloy. *Prog. Nat. Sci. Mater. Int.* **2016**, *26*, 391–397. [\[CrossRef\]](#)
13. Birol, Y. Microstructural evolution during annealing of a rapidly solidified Al–12Si alloy. *J. Alloy. Compd.* **2007**, *439*, 81–86. [\[CrossRef\]](#)
14. Farag, O.F. Comparison of the Effect of Plasma Treatment and Gamma Ray Irradiation on PS-Cu Nanocomposite Films Surface. *Results Phys.* **2018**, *9*, 91–99. [\[CrossRef\]](#)
15. Wei, D.; Wang, X.; Wang, R.; Cui, H. Surface modification of 5CrMnMo steel with continuous scanning electron beam process. *Vacuum* **2018**, *149*, 118–123. [\[CrossRef\]](#)
16. Zaguliaev, D.V.; Ivanov, Y.F.; Klopotov, A.A.; Ustinov, A.M.; Shlyarov, V.V.; Yakupov, D.F. Evolution of strength properties and defect sub-structure of the hypoeutectic A319.0 alloy irradiated by a pulsed electron beam and fractured under tensile stress. *Materialia* **2021**, *20*, 101223. [\[CrossRef\]](#)
17. Zaguliaev, D.; Ivanov, Y.; Konovalov, S.; Shlyarov, V.; Yakupov, D.; Leonov, A. Effect of pulsed electron beam treatment on microstructure and functional properties of Al-5.4Si-1.3Cu alloy. *Nucl. Instrum. Methods Phys. Res. Sect. B Beam Interact. Mater. At.* **2021**, *488*, 23–29. [\[CrossRef\]](#)
18. Kang, N.; Mansori, M.E.L. A new insight on induced-tribological behaviour of hypereutectic Al-Si alloys manufactured by selective laser melting. *Tribol. Int.* **2020**, *149*, 105751. [\[CrossRef\]](#)
19. Zaguliaev, D.; Gromov, V.; Rubannikova, Y.; Konovalov, S.; Ivanov, Y.; Romanov, D.; Semin, A. Structure and phase states modification of AL-11SI-2CU alloy processed by ion-plasma jet and pulsed electron beam. *Surf. Coat. Technol.* **2020**, *383*, 125246. [\[CrossRef\]](#)
20. Ivanov, Y.; Gromov, V.; Zaguliaev, D.; Glezer, A.; Sundeev, R.; Rubannikova, Y.; Semin, A. Modification of surface layer of hypoeutectic silumin by electroexplosion alloying followed by electron beam processing. *Mater. Lett.* **2019**, *253*, 55–58. [\[CrossRef\]](#)
21. Romanov, D.A.; Budovskikh, E.A.; Zhmakin, Y.D.; Gromov, V.E. Surface modification by the EVU 60/10 electroexplosive system. *Steel Transl.* **2011**, *41*, 464–468. [\[CrossRef\]](#)
22. Koval, N.N.; Ivanov, Y.F. *Electron-Ion Plasma Modification of the Surface of Nonferrous Metals and Alloys*; Publishing House of Scientific and Technology Literature: Tomsk, Russia, 2016; p. 304.
23. Gromov, V.E.; Zagulyaev, D.V.; Ivanov, Y.F.; Konovalov, S.V.; Nevsky, S.A.; Sarychev, V.D.; Budovskikh, E.A.; Rubannikova, Y.A. *Structure and Hardening of Silumin Modified by Electron-Ion Plasma*; SibGIU: Novokuznetsk, Russia, 2020; p. 285.
24. Egerton, F.R. *Physical Principles of Electron Microscopy*; Springer International Publishing: Basel, Switzerland, 2016; p. 196.
25. Kumar, C.S.S.R. *Transmission Electron Microscopy. Characterization of Nanomaterials*; Springer: New York, NY, USA, 2014; p. 717.
26. Carter, C.B.; Williams, D.B. *Transmission Electron Microscopy*; Springer International Publishing: Cham, Switzerland, 2016; p. 518.
27. Ivanov, Y.F.; Zagulyaev, D.V.; Nevskii, S.A.; Gromov, V.E.; Sarychev, V.D.; Semin, A.P. Microstructure and properties of hypoeutectic silumin treated by high-current pulsed electron beams. *Prog. Phys. Met.* **2019**, *20*, 447–484. [\[CrossRef\]](#)

28. Zaguliaev, D.; Konovalov, S.; Ivanov, Y.; Abaturova, A.; Leonov, A. Microstructure and Microhardness of Piston Alloy Al-10Si-2Cu Irradiated by Pulsed Electron Beam. *Arch. Foundry Eng.* **2020**, *20*, 92–98.
29. Bannykh, O.A.; Budberg, P.B.; Alisova, S.P.; Guzey, L.S.; Drits, M.E.; Dobatkina, T.V.; Lysova, E.V.; Nikitina, N.I.; Padezhnova, E.M.; Rokhlin, L.L.; et al. *State Diagrams of Binary and Multicomponent Systems Based on Iron*; Metallurgy: Moscow, Russia, 1986.
30. Utevsky, L.M. *Diffraction Electron Microscopy in Metal Science*; Metallurgy: Moscow, Russia, 1973; p. 584.
31. Thomas, G.; Goringe, M.J. *Transmission Electron Microscopy of Materials*; Nauka: Moscow, Russia, 1983; p. 320.